A novel cholesterol stain reveals early neuronal cholesterol accumulation in the Niemann-Pick type C1 mouse brain

Patrick C. Reid,* Naomi Sakashita,* Shigeki Sugii,* Yoshiko Ohno-Iwashita,[†] Yukiko Shimada,[†] William F. Hickey,[1,§] and Ta-Yuan Chang[1,*]

Department of Biochemistry,* Dartmouth Medical School, Hanover, NH 03755; Biomembrane Research Group,[†] Tokyo Metropolitan Institute of Gerontology, 35-2 Sakae-cho, Itabashi-ku, Tokyo 173-0015, Japan; and Department of Pathology,[§] Dartmouth Medical School, Hanover, NH 03755

Abstract Niemann-Pick type C (NPC) is a neurodegenerative disorder characterized by progressive accumulation of cholesterol, gangliosides, and other lipids in the central nervous system and visceral organs. In the NPC1 mouse model, neurodegeneration and neuronal cell loss occur before postnatal day 21. Whether neuronal cholesterol accumulation occurs in vivo before the first signs of neuronal cell loss has not been demonstrated. In this report, we used the NPC1 mouse model and employed a novel cholesterol binding reagent, BCθ, that enabled us to visualize cellular cholesterol accumulation at a level previously unattainable. ■ The results demonstrate the superiority of BCθ staining over conventional filipin staining in confocal microscopy and highlight several new findings. We show that at postnatal day 9, although only mild signs of neurodegeneration are detectable, significant neuronal cholesterol accumulation has already occurred throughout the NPC1 brain. In addition, although NPC1 Purkinje neurons exhibit a normal morphology at day 9, significant cholesterol accumulation within their extensive dendritic trees has occurred. We also show that in the thalamus and cortex of NPC1 mice, activated glial cells first appear at postnatal day 9 and heavily populate by day 22, suggesting that in NPC1 mice, neuronal cholesterol accumulation precedes neuronal injury and neuronal cell loss.—Reid, P. C., N. Sakashita, S. Sugii, Y. Ohno-Iwashita, Y. Shimada, W. F. Hickey, and T-Y. Chang. **A novel cholesterol stain reveals early neuronal cholesterol accumulation in the Niemann-Pick type C1 mouse brain.** *J. Lipid Res.* 2004. 45: 582–591.

Supplementary key words intracellular cholesterol accumulation • Niemann-Pick Disease • neuron • astrocyte • Purkinje cell • neurodegeneration • BCθ

Niemann-Pick type C (NPC) disease is a fatal autosomal recessive neurovisceral disorder in humans and in animals, characterized by progressive neurodegeneration in the central nervous system (CNS) and hepatosplenomegaly. The disease can be caused by mutations in one of two genes, NPC1 and NPC2 [as reviewed in ref. (1)]. Mutations in *Npc1* account for 95% of all NPC disease cases, whereas mutations in *Npc2* account for the remaining 5% (1). At the cellular level, NPC disease is characterized by the accumulation of unesterified cholesterol, sphingomyelin, glycosphingolipids, and other lipids within the endosomal/lysosomal system in various tissues. The *Npc1* gene encodes a multi-pass transmembrane protein with a putative sterol-sensing domain (2). It resides within the tubulovesicles associated with the late endosome/lysosome (3, 4). In NPC1 mutant cells, the transport of both LDL-derived and endogenously synthesized cholesterol through the endosome/lysosome is partially defective in a cell type-dependent manner (5–10). NPC1 may be required for vesicular shuttling of both membrane lipids and fluid phase constituents from the late endosome to various destinations (11, 12). In vitro, the NPC1 protein exhibits a transmembrane molecular pump activity for fatty acids but not for cholesterol (13). The *Npc2* gene encodes the soluble protein HE1, a lysosomal protein that can be secreted into the growth medium (14). NPC2 binds cholesterol with very high affinity and binds fatty acids with lower affinity (15).

Despite evidence at the in vitro level favoring the view that NPC1 and NPC2 are involved in intracellular cholesterol transport, the direct connection between cholesterol accumulation and neurodegeneration in NPC brains remains under debate. Earlier studies [as reviewed in ref. (1)] reported that glycolipids are elevated in the NPC1 brain, the primary target of this disease, whereas there is

---

Abbreviations: CNS, central nervous system; GFAP, glial fibrillary acidic protein; NPC, Niemann-Pick type C; PM, plasma membrane; WT, wild-type.
[1] To whom correspondence should be addressed.
  e-mail: Ta.Yuan.Chang@Dartmouth.edu (T-Y.C.);
  William.F.Hickey@Dartmouth.edu (W.F.H.)

no overt increase in cholesterol in the brain in human NPC1 or its animal models (16). The neuropathological abnormalities of NPC1 disease resemble those in primary gangliosidoses (i.e., diseases caused by enzyme deficiencies in the glycolipid degradation pathway). The connection between glycolipids and NPC1 is further supported by the work of Vanier (17), who reported that the total GM2 and GM3 contents in the cerebral cortex of a three-month-old patient were highly elevated as compared with those of age-matched infants. In addition, Zervas, Dobrenis, and Walkley (18) used a monoclonal antibody against GM2 to perform immunostaining and showed that the GM2 immunoreactivity increased in the cortical pyramidal neurons in animals and humans with NPC1 in a manner similar to that found in primary GM2 gangliosidosis. The same group of investigators then showed that treating NPC1 animals with the drug *N*-butyldeoxynojirimycin, an inhibitor of the enzyme glucosylceramide synthase, a key enzyme in the early glycosphingolipid biosynthesis pathway, decreased the ganglioside accumulation and the accompanying neuropathological changes in their brains (19). These and other studies suggested that NPC1 might be considered a glycolipid storage disease rather than a cholesterol storage disease.

However, recent evidence for cholesterol accumulation in the NPC1 brain has been described. In NPC1 mice, Zervas, Dobrenis, and Walkley (18) reported cholesterol accumulation in various neurons, in addition to GM2 accumulation. The mice examined by these investigators were at 9.5 weeks of age, and were near the end of their life span (which averages between 10 to 11 weeks) (1). In a separate study, Treiber-Held et al. (20) examined cholesterol accumulation in NPC1 mice between 3 and 10 weeks of age. They reported significant cholesterol accumulation in neurons of the cortex, the CA1 region of the hippocampus, and the cerebellar cortex as early as 3 weeks of age (20). In addition, they observed only mild cholesterol accumulation in the CA3 region of the hippocampus, the dentate gyrus, and the thalamus. However, in the NPC1 mouse, neurodegeneration and low levels of neuronal cell loss have been reported to occur before postnatal day 21, with the earliest signs of neurodegeneration reported at postnatal day 9 (21, 22). In addition, by day 21 there is already a 13% loss of Purkinje neurons from the cerebellum, a hallmark of NPC disease, which progresses to a 98% loss by the end of the life span (22). Whether significant cholesterol accumulation occurs in vivo before the first signs of neuronal cell loss (pre-postnatal day 21) and neurodegeneration has not been demonstrated.

To visualize cholesterol accumulation in cells, various investigators invariably use filipin staining as the standard method [as reviewed in ref. (1)]. Filipin binds to cholesterol with high affinity; however, it exhibits rapid photobleaching and only modest natural fluorescence under UV excitation, making its detection under confocal microscopy difficult. Recently, a novel method for detecting cholesterol-rich domains utilizing the cholesterol binding agent BCθ was developed. BCθ originates from a protein toxin called theta-toxin produced by *Clostridium perfrin-*

gens. For detection purposes, the toxin has been modified by proteolysis and then biotinylated. By employing avidin-conjugated fluorescent dyes, BCθ bound to cellular cholesterol can be visualized under fluorescence microscopy (23). In unfixed cells or cells fixed with 1% or 2% paraformaldehyde, BCθ cannot enter the cell interior and binds mainly to cholesterol-rich domain(s) at the cell surface (24, 25). In contrast, when cells are fixed with 4% paraformaldehyde, a significant portion of the cholesterol binding sites at the plasma membrane (PM) are inactivated, presumably because of extensive cross-linking of membrane proteins (26). Concurrently, the cells become leaky to various macromolecules, allowing BCθ to enter the cell interior. At the cell interior, BCθ was shown to stain mainly cholesterol-rich domains; the complexes formed can be visualized under fluorescence microscopy in a manner far superior to that of filipin (25). In the current study, we employ this new method to monitor cholesterol accumulation in the brains of NPC1 mice from the first signs of neurodegeneration at postnatal day 9 to a stage of low levels of neuronal cell loss at postnatal day 22.

MATERIALS AND METHODS

Animal and tissue preparations

The animal studies were prereviewed and approved by the Institutional Animal Use and Care Committee at Dartmouth College, Hanover, New Hampshire: Protocol #11601. The BALB/c NPC1[NIH] mice were kindly donated by Peter G. Pentchev at the National Institutes of Health. Mice were bred as NPC^{+/−} heterozygotes. Litters were genotyped via tail snip DNA by a previously described PCR method (27). Preliminary studies revealed no detectable abnormal phenotypes in the heterozygous animals (NPC^{+/−}), consistent with previous reports. Homozygous NPC (NPC^{−/−}) mice and their age-matched normal siblings (NPC^{+/+}) were examined at 9, 11, 15, and 22 days of age, with n = 4 animals (2 NPC^{−/−} and 2 NPC^{+/+}) per age point. At each time period, mice were anesthetized with ether and perfused through their hearts with Dulbecco's phosphate buffered saline without calcium and magnesium followed by 4% paraformaldehyde in 0.1 M phosphate buffer (pH 7.4). The brains were excised, and large coronal sections were taken with a razor blade through the cerebellum and the underlying brain stem, and through the cortex and the underlying basal structures. The large tissue sections were fixed in 4% paraformaldehyde for 30 min, washed multiple times in 0.2 M phosphate buffer, and cryoprotected in 30% sucrose at 4°C overnight. For each animal, coronal brain sections from the cerebellum/brainstem and the cortex/basal structures were embedded side by side; 5 μm thin sections were cut on a cryostat and placed on precleaned glass slides. Section slides were blocked with 1% fetal bovine serum (FBS) in 0.5 M Tris (pH 7.6), or with PBS containing 1% BSA and the nonspecific mouse IgM antibodies (for GM1 and GM2 slides only), then stained for histochemical analysis as described below.

Histochemical analysis

Section slides described above were incubated overnight at 4°C on humidified trays with various primary staining reagents diluted in 0.5 M Tris containing 1% FBS, or in PBS containing 1% BSA (for GM1 and GM2 staining). BCθ was prepared as previously described (24) and used at 15 μg/ml. Anti-GM1 biotin-

conjugated mouse monoclonal class IgM was from Seikagaku Co., Japan, and was used at 1:100 (v/v). Anti-GM2 mouse monoclonal class IgM, described by Taniguchi et al. (28), was generously provided by Dr. T. Tai of the Tokyo Metropolitan Institute of Gerontology. For GM1 and GM2 staining, sections were permeabilized with 0.5% Triton X-100 as described previously (28). Filipin (125 µg/ml) staining was performed under light-protected conditions for 2 h at room temperature, as previously described (25). After incubation with primary reagents, slides were washed with 0.5 M Tris containing no FBS and counterstained with Neurotrace™ fluorescent Nissl Stain (N-21480) 500/525 green (Molecular Probes, Eugene, OR) according to the manufacturer's literature. Anti-Calbindin-D-28K (EG-20) rabbit polyclonal antibodies (Sigma) were used to stain Purkinje neurons and their dendritic architecture. Anti-glial acidic fibrillary protein (GFAP) rabbit polyclonal antibodies (Sigma) were used to stain reactive astrocytes. Anti-F4/80 rat monoclonal antibodies (Accurate Chemical and Scientific Corp.) were used to stain macrophages. Bound BCθ, GM1, GM2, GFAP, or Calbindin antibodies were detected with the following secondary reagents: streptavidin-Alexa 488 or -Alexa 568 (at 1:1,000, v/v), goat anti-mouse IgM-Alexa 647 (at 1:150, v/v), horse/goat anti-rabbit-Alexa 488 (at 1:150, v/v), -Alexa 568 (at 1:150, v/v), or Cy 5 (at 1:150, v/v), and donkey anti-rat-Alexa 568 (at 1:150, v/v). All secondary reagents were from Molecular Probes. Slides were treated with Prolong anti-fade from Molecular Probes. Images were collected with a confocal microscope (Bio-Rad MRC-1024) and constructed with LaserSharp software. Images of filipin-stained sections were collected on a Leica TCS-SP confocal microscope equipped with an argon laser for UV excitations, and constructed with Leica Confocal Software.

Quantification of cholesterol accumulation by BCθ

Multiple coronal brain sections from postnatal day 9, 11, 15, and 22 NPC and wild-type (WT) mice were stained with BCθ and Neurotrace. Sections representing cortex, thalamus, hypothalamus, hippocampus, dentate gyrus, and cerebellum were examined under a 10× objective using a Bio-Rad MRC1024 confocal microscope. For each section, six image scans, encompassing all regions of the brain, were taken, and the total image BCθ fluorescent intensity was determined by LaserSharp software. The Alexa dye conjugates used are very photo-stable under confocal microscopy, and no reduction in signal was observed during analysis. Sections from WT mice exhibited low levels of BCθ-positive signals, representing background staining of synaptosomal membranes and myelin-associated cholesterol. Therefore, to serve as a baseline, we adjusted the IRIS and GAIN features of the MRC1024 confocal microscope so that WT day 9 brain sections exhibited mean fluorescent intensities of 1,000 arbitrary units. Once these parameters were set, sections from WT day 11, 15, and 22 and NPC day 9, 11, 15, and 22 mice were scanned and the intensity values measured. To ensure that the measured intensity values were proportional to the signal intensity, instrument settings were chosen such that the signals recorded from the brightest samples prepared from the NPC1 mice did not go beyond the full-scale value. To confirm these findings, in a second experiment, a second set of brains from NPC and WT day 9, 11, 15, and 22 mice was examined in the same manner. Neurotrace staining was used to aid in the identification of regions and as an internal standard to determine differences in staining intensities in NPC and WT sections. Measurements of neurotrace fluorescent intensities showed <15% difference in values, indicating that the differences were specific to BCθ staining. Attempts to perform a similar analysis with filipin proved impossible because of the high background associated with filipin staining at these ages and its rapid bleaching time in confocal microscopy.

RESULTS

To compare the ability of BCθ and filipin to detect cholesterol accumulation in vivo, normal (WT) and NPC1 (NPC) mouse brains, taken from postnatal day 9, 15, and 22 genotype-confirmed animals were processed for histochemistry and stained with BCθ and with filipin in parallel. A fluorescent Nissl stain, Neurotrace™ (Molecular Probes), which stains the extensive rough endoplasmic reticulum in neurons, was used as an identifying marker for neurons. As early as postnatal day 9, positive BCθ staining (**Fig. 1**, arrows), indicative of cholesterol accumulation, was observed in neurons of all regions of the NPC brain, including the cerebellum, cortex, thalamus, granule layer of the dentate gyrus, and the large pyramidal neurons of Ammon's horn in the hippocampus (regions CA1–CA3). This staining was variable from region to region, but in general, the extent of cholesterol accumulation progressed from day 9 to day 22. In WT mouse brains, cholesterol accumulation was undetectable in these regions. In comparison, weak sporadic filipin staining (**Fig. 2**) in neurons was present in postnatal day 9 NPC brains, with increased signals observed in NPC brains at postnatal day 22, although both NPC and WT brains exhibited high background (Fig. 2).

In NPC cerebellum, BCθ staining detected low levels of cholesterol accumulation within Purkinje cells (Fig. 1, arrows; CBL indicated by the asterisk) and small granule neurons (Fig. 1; CBL, indicated by the plus sign) of the granule layer as early as postnatal day 9. Cholesterol accumulation in both Purkinje and granule neurons increased from day 9 to day 22 (Fig. 1, CBL). In WT mouse brain, BCθ did not detect any cholesterol accumulation between day 9 and day 22 within the cerebellum (Fig. 1, CBL). In contrast, cholesterol accumulation could not be detected by filipin in postnatal day 9 NPC cerebellum (Fig. 2, CBL). By day 22, filipin staining could detect cholesterol accumulation within Purkinje neurons (Fig. 2, arrows; CBL, asterisk), but not in granule neurons. At day 9, based on morphological appearance, NPC Purkinje cells exhibited no obvious abnormalities, but by day 22, multiple alterations in cell morphology, such as dendritic alterations and axonal swelling, became visually apparent. In addition, there was evidence of missing Purkinje cells when NPC cerebellar sections were stained with Calbindin, a Purkinje cell marker protein, suggesting initial Purkinje cell loss. At this stage, neuronal cell loss in the granular layer was not obvious.

In NPC cortex (Fig. 1, CTX), at day 9, significant cholesterol accumulation was observed in neurons of all layers. Accumulation occurred predominantly in the neuronal perikarya (asterisk) as well as the axon hillock region (arrow). Cholesterol accumulations were barely detectable by filipin staining at postnatal day 9, and were difficult to discern from background staining (Fig. 2, CTX). Filipin staining at day 22 showed cholesterol accumulations in the axon hillock region of most neurons (Fig. 2, CTX, indicated by arrows), similar to BCθ staining. Morphologically, early signs of neuronal swelling in the cortex became visible by day 22.
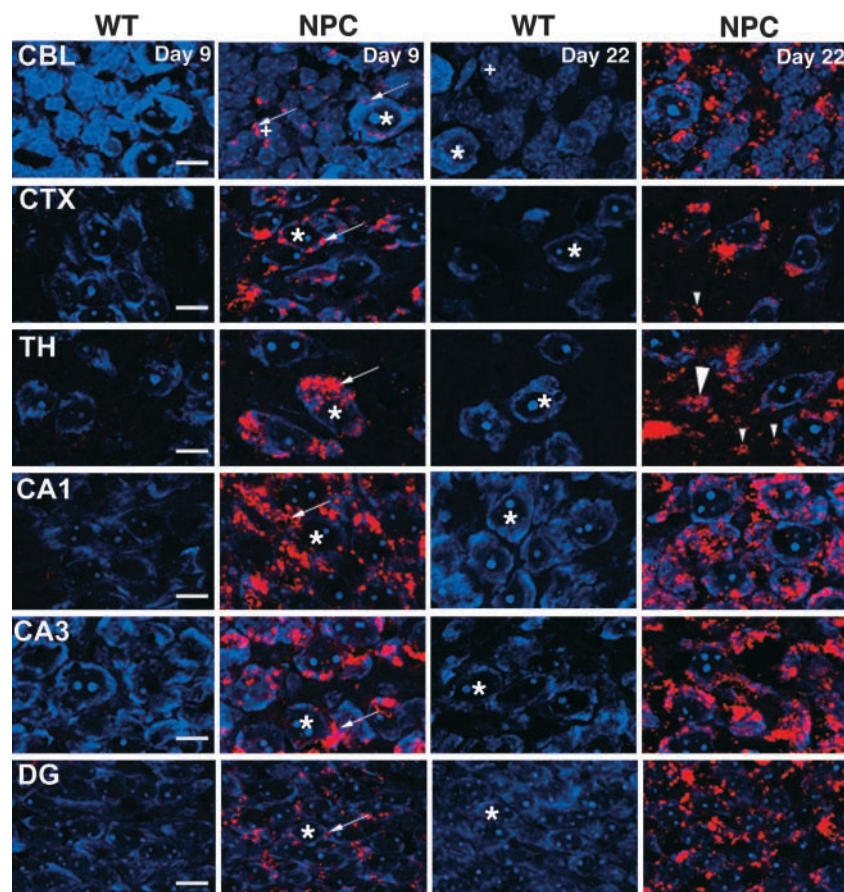
Fig. 1. Detection of neuronal cholesterol accumulation by BCθ staining. Coronal brain sections (5 μm) taken from sibling wild-type (WT) (NPC1$^{+/+}$) and NPC (NPC1$^{-/-}$) mice perfuse-fixed with 4% paraformaldehyde were stained with BCθ (red) and neurotrace (blue), and examined by confocal microscopy. BCθ (red) stains intracellular cholesterol-rich domain(s), indicated by arrows; neurotrace (blue), a fluorescent Nissl stain, stains neuronal perikarya, indicated by asterisks. Images shown are high-magnification images obtained from WT and Niemann-Pick type C (NPC) brains at postnatal days 9 and 22 and are representative of a large number of photographs obtained by confocal microscopy from multiple day 9, 11,15, and 22 WT and NPC mice brains. Abbreviations used: CBL, cerebellum; CTX, cortex; TH, thalamus; CA1, hippocampus CA1 region; CA3, hippocampus CA3 region; DG, dentate gyrus. Scale bars are 10 μm.

The NPC thalamus (Fig. 1, TH) at day 9 exhibited the most severe BCθ staining, representing massive cholesterol accumulation per neuron. Cholesterol accumulated in the neuronal perikarya and at the base of the perikarya/axon hillock (Fig. 1, TH, arrow). A similar finding had previously been reported in 9.5-week NPC1 mice (17). Only mild filipin staining was observed in NPC thalamus between days 9 and 22 (Fig. 2, TH). Those neurons (asterisk) that did stain positive for filipin (arrow) exhibited a staining pattern similar to that observed for BCθ staining. Morphologically, the NPC thalamus appeared normal at postnatal day 9, but by day 22, degenerating neurons (Fig. 1, TH, large arrowhead) contained large amounts of cholesterol. In addition, a number of apparent degenerating terminals (Fig. 1, TH, small arrowheads) could be observed.

Between days 9 and 22, the NPC hippocampus showed massive cholesterol accumulation (Fig. 1, HC), predominantly in the large pyramidal neurons of Ammon's horn, throughout the CA1 and CA3 regions. During this time

period, no obvious signs of neuronal cell loss in any region of the hippocampus were observed. Only mild filipin staining could be detected at day 9 in the CA3 region (Fig. 2, HC); however, the signals became easily detectable at day 22 (Fig. 2, HC, arrow). Interestingly, filipin staining in the CA1 region of the hippocampus was sporadic even at day 22, and was difficult to discern from background staining (data not shown). This finding is consistent with that of Treiber-Held et al. (20), who reported reduced filipin staining in the CA1 region compared with the CA3 region of the NPC hippocampus. In the NPC dentate gyrus, BCθ staining by day 22 was intense in the small neurons of the granular layer (Fig. 1, DG, arrow), whereas only sporadic staining was observed in neurons of the polymorph layer (data not shown). Filipin staining could not detect cholesterol accumulation at day 9 in the NPC dentate gyrus, and even by day 22, only a few neurons stained filipin-positive for cholesterol accumulation (Fig. 2, DG, arrow, asterisk).

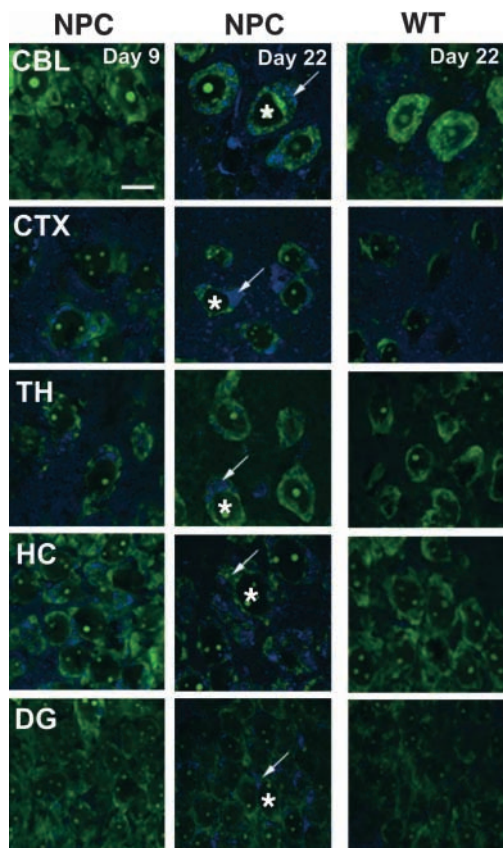The stable fluorescent signal of Alexa® BCθ staining allowed us to quantify cholesterol accumulation in the NPC

Fig. 2. Detection of neuronal cholesterol accumulation by filipin staining. Coronal brain sections (5 µm) taken from sibling WT (NPC1$^{+/+}$) and NPC (NPC1$^{-/-}$) mice perfuse-fixed with 4% para-formaldehyde were stained with filipin (blue) and neurotrace (green) and examined by confocal microscopy. Filipin (blue) stains intracellular cholesterol-rich domain(s), indicated by arrows; neurotrace (green), a fluorescent Nissl stain, stains neuronal perikarya, indicated by asterisks. Images shown are high-magnification images obtained from WT and NPC brains at postnatal days 9 and 22, and are representative of a large number of photographs obtained by confocal microscopy from multiple day 9, 11, 15, and 22 WT and NPC mice brains. Abbreviations used: CBL, cerebellum; CTX, cortex; TH, thalamus; HC, hippocampus CA3 region; DG, dentate gyrus. Scale bar is 10 µm.
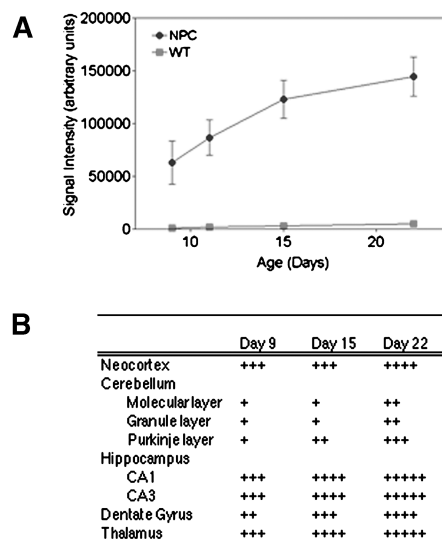

Fig. 3. Quantification of cholesterol accumulation in the NPC mouse brain by BCθ staining. Coronal brain sections from days 9, 11, 15, and 22 WT and NPC mice were stained with BCθ and neurotrace and analyzed by confocal microscopy. BCθ signal intensities were measured as described in Materials and Methods. A: Accumulation of cholesterol between postnatal days 9 and 22, as detected by BCθ staining, in WT (squares) and NPC (circles) mice brains. Each data point represents the mean ± SD of twelve BCθ intensity scans taken from two mice. B: Regional distribution of cholesterol accumulation, as detected by BCθ staining, in the NPC mouse brain.

brain by measuring BCθ signal intensity (see Materials and Methods). In two independent experiments, sections from WT and NPC day 9, 11, 15, and 22 brain sections were scanned and the BCθ signal intensity values measured (**Fig. 3A**). These results show a significant increase in cholesterol accumulation in the NPC brain between postnatal day 9 and day 15; the increase in cholesterol accumulation appears to slow down between day 15 and day 22. In WT control sections, virtually no cholesterol accumulation was observed between day 9 and day 22. The dramatic increase in cholesterol accumulation in the NPC brain was observed throughout the various regions and to varying extents (Fig. 3B).

To examine cholesterol accumulation in Purkinje neurons, cerebellar sections from postnatal day 9, 15, and 22 WT and NPC mice were immunohistochemically stained for calbindin (**Fig. 4**, blue), a Purkinje cell marker protein,

and costained with BCθ (Fig. 4, red) to detect cholesterol accumulations. As early as postnatal day 9, punctate cholesterol accumulations could be observed in NPC Purkinje cell bodies (Fig. 4, asterisk). In addition, we observed significant cholesterol accumulation within the extensive dendritic arbors of NPC Purkinje neurons (Fig. 4, arrows). The majority of cholesterol accumulated in a punctate pattern and was localized in the main dendritic branch originating from the NPC Purkinje cell body (arrows). Scanning of various Z-sections of this main dendritic branch by confocal microscopy confirmed that the cholesterol accumulation was inside the NPC dendrite (data not shown). This BCθ staining was specific to NPC, inasmuch as WT Purkinje dendrites exhibited no positive BCθ signals (Fig. 4). Although the majority of BCθ-positive signals colocalized with calbindin, those that did not were determined to be associated with degenerated synaptic connections (synaptophysin-positive), other neurons (Neurotrace-positive) of the molecular layer, and/or glial cells (GFAP-positive) (data not shown). In WT sections, BCθ staining did not detect intracellular cholesterol accumulation in either Purkinje cell bodies or dendrites, and did not detect accumulations associated with other cells of the cerebellum (Fig. 4, Fig. 1, CBL).

The presence of reactive astrocytes represents one of the earliest indications of various neuronal injury events and often occurs well before morphological alterations in neurons become detectable. In both NPC patients and NPC mice, the thalamus exhibits severe neurodegeneration during the early onset of the disease (1, 21). To monitor the presence of reactive astrocytes in NPC mouse thal-
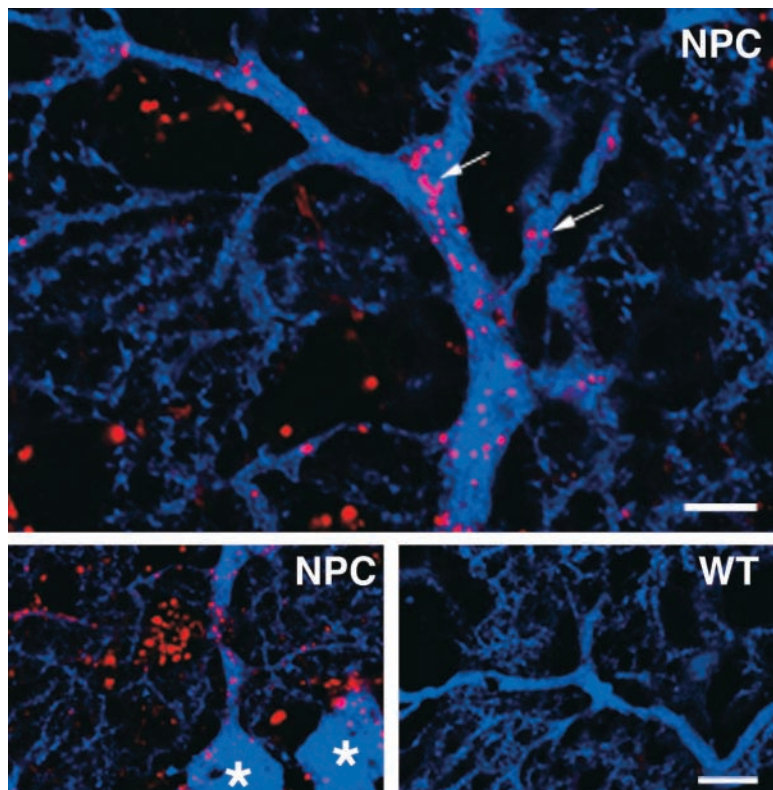
Fig. 4. Early cholesterol accumulation occurs in dendrites of NPC Purkinje neurons. Cerebellar brain sections (5 μm) from postnatal days 9, 15, and 22 WT and NPC mice were stained with BCθ (red) and anti-Calbindin antibodies (blue; a Purkinje cell marker protein). Images shown are of postnatal day 9 cerebellar sections from NPC (main panel, Purkinje dendrite, cholesterol accumulation indicated by arrows, scale bar is 5 μm; lower left panel, Purkinje cell body, indicated by asterisk, scale bar is 10 μm) and WT (lower right panel, Purkinje dendrite, scale bar is 10 μm) mice brains. Images are representative of similar data obtained in WT and NPC mice brains at postnatal days 15 and 22.

amus, we performed double staining using BCθ (red) and antibodies against the GFAP (green), a protein marker for reactive astrocytes (**Fig. 5**). The results show that by day 9, most neurons accumulated large amounts of intracellular cholesterol (Fig. 5A, red; arrowhead), whereas only a few reactive astrocytes (Fig. 5A, green; arrow) were present. The amount of reactive astrocytes increased significantly by day 15, and by day 22, dense astrogliosis occurred throughout the area. By day 22, astrocyte activation was also observed in the cortex, whereas in the hippocampus and cerebellum, astrocyte accumulation was only sporadic (data not shown). In addition, the appearance of macrophages (in low numbers) occurred throughout the thalamus and cortex (results not shown). In normal mice, neither intracellular cholesterol nor reactive astrocytes were present in any of these regions between days 9 and 22. In addition, reactive astrocytes in the NPC1 brains exhibited progressive cholesterol accumulation (Fig. 5B). In these activated astrocytes, cholesterol accumulations were detected within the main body of the astrocyte (Fig. 5B, large arrowheads) and within their processes (Fig. 5B, large arrows).

In addition to cholesterol accumulation, we examined GM1 and GM2 accumulation in postnatal days 9 and 22 WT and NPC mice brains. At postnatal day 22, we observed comparable levels of GM1 and GM2 immunoreactivity in various neurons from WT and NPC1 mice brains (**Fig. 6**). In general, the GM1 signal localized predominantly to neuronal synaptosomal membranes (Fig. 6A, arrows), a finding confirmed by immunohistochemical analysis of the synaptosomal membrane protein, synaptophysin (data not shown). Neurons from the cerebellum, including Purkinje neurons (Fig. 6A, CBL, asterisk),

the thalamus (Fig. 6A; TH, arrowheads), the cortex, and the pyramidal layer of the hippocampus (results not shown) were examined. In non-neuronal cells, a significant increase in GM1 immunoreactivity (arrows) was observed in reactive astrocytes that accumulated in thalamus, cortex, and other regions of the NPC1 mice brains. An example is shown in Fig. 6A, TH, row 4. Interestingly, we found that GM1 accumulation occurred not only in activated NPC astrocytes (GFAP, blue), but also in the few sporadic activated WT astrocytes (Fig. 6A; row 4, arrows) found. Parallel experiments using mice at postnatal day 9 produced similar results, with no significant difference in GM1 staining observed between WT and NPC mice (results not shown). For GM2, in day 22 NPC1 mice brains, a slight increase in immunoreactive signal could be observed within neurons of the thalamus (Fig. 6B; TH, asterisk) and neurons in various other regions (results not shown). In addition, a significant increase in GM2 signal could be observed in macrophages (F4/80, macrophage marker, blue) in the thalamus and cortex (Fig. 6B; bottom panel, GM2, green, arrowheads). Parallel experiments using mice at postnatal day 9 showed no significant difference in GM2 staining between WT and NPC mice (results not shown). Thus, by postnatal day 22, the NPC brain showed no significant accumulation of GM1 within neurons but did show a significant increase in GM1 immunoreactivity in the large number of reactive astrocytes present (Figs. 5A, 6). In addition, NPC brain exhibited only a minor accumulation of GM2 in neurons compared with WT, but did show significant increases in GM2 immunoreactivity in macrophages. These findings are largely consistent with the early study by Taniguchi et al. (28).
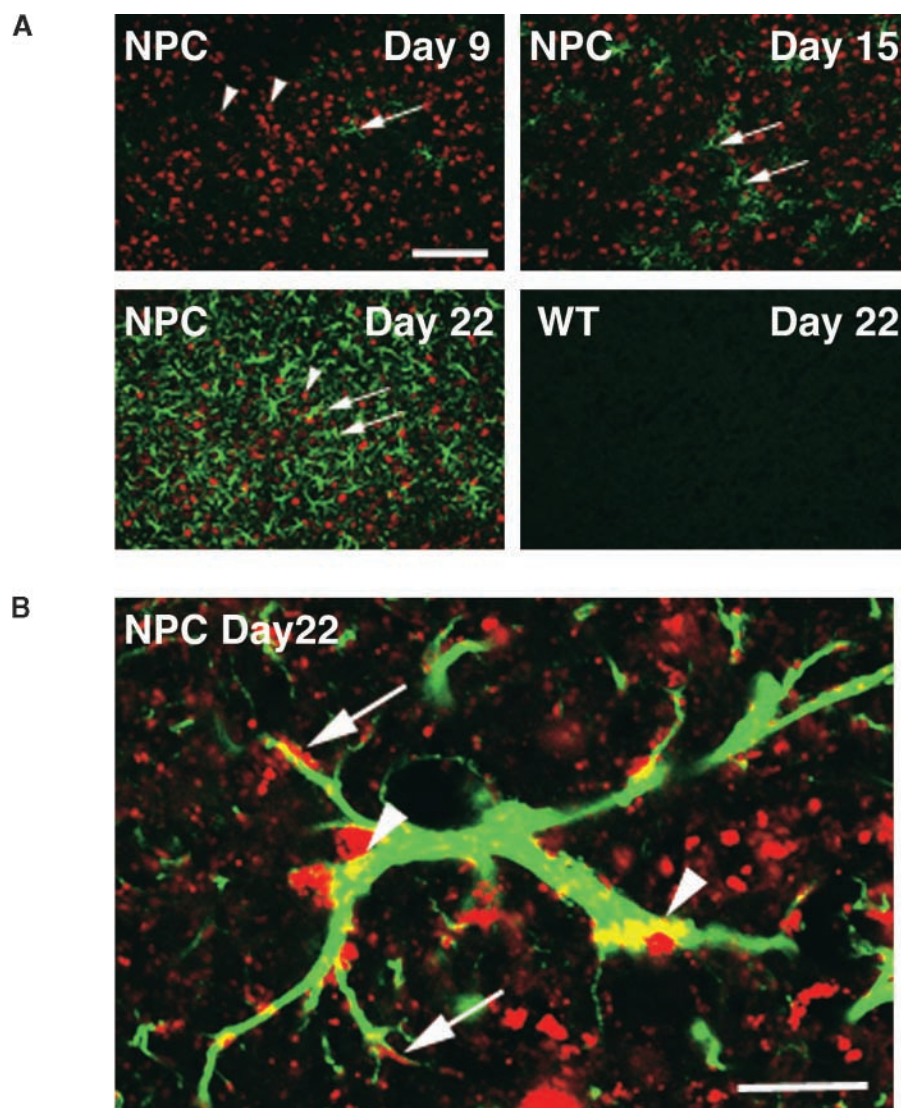
Fig. 5. Neuronal cholesterol accumulation precedes astrocyte activation in the NPC mouse brain. Coronal brain sections (5 μm) from postnatal days 9, 15, and 22 WT and NPC mice were stained with BCθ (red) and anti-glial fibrillary acidic protein (GFAP) antibodies (green; an activated astrocyte marker protein). A: Cholesterol accumulation in neurons (red, arrowheads) precedes astrocyte activation (green, arrows). Images shown are from NPC thalamus at days 9, 15, and 22, and control WT thalamus at day 22. Scale bar is 100 μm. B: Cholesterol (red) accumulates in the main body (large arrowheads) and processes (large arrows) of activated NPC astrocytes. Image is of a day 22 activated NPC astrocyte. Scale bar is 10 μm. Images are representative of a large number of photographs obtained by confocal microscopy.

DISCUSSION

In this report, we demonstrate that the new cholesterol staining reagent, BCθ, can detect intracellular cholesterol accumulations in vivo at a level far superior to that achieved by conventional filipin staining. Interestingly, the comparison of BCθ to filipin for the detection of cholesterol accumulation in the NPC mouse brain revealed significant differences between these two reagents. As early as postnatal day 9, clear BCθ-positive signals were observed in almost 90% of neurons throughout the NPC brain, with the intensity increasing up to day 22. In contrast, filipin-positive signals were detected in only cortex, thalamus, and the hippocampus at day 9, and only in 30% to 50% of the neurons in these regions. By day 22, filipin-positive signals were in all brain regions, with 40% to 80% of the neurons exhibiting some positive filipin staining. This finding suggests that compared with BCθ staining, cells must accumulate a higher threshold level of cholesterol before they stain filipin-positive.

Recently, Treiber-Held et al. (20) reported the spatial and temporal (3–10 weeks) accumulation of free cholesterol in the NPC mouse brain detected by filipin staining. At the preclinical age of 3 weeks, they reported interneuronal storage of cholesterol in the cerebral cortex, the CA3 region of the hippocampus, and the cerebellum, but little cholesterol accumulation in the CA1 region of the hippocampus, the granular layer of the dentate gyrus, and
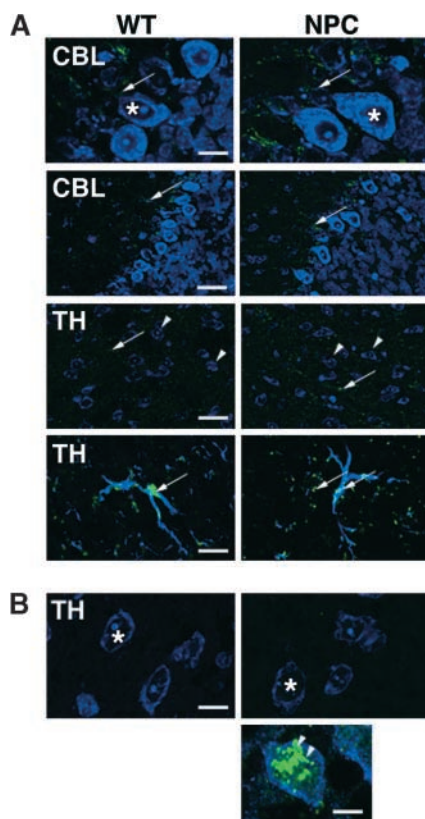
Fig. 6. Ganglioside (GM1 and GM2) accumulation in WT and NPC mice brains. A: Coronal brain sections (5 μm) from days 9 and 22 WT and NPC mice were stained with anti-GM1 antibodies (green) and neurotrace (blue) (rows 1–3) or GFAP (blue) (row 4). Row 1: high-magnification images from the cerebellum (CBL); Purkinje neurons indicated by asterisk, GM1 synaptosomal staining indicated by arrows. Scale bar is 10 μm. Row 2: low-magnification images of the same CBL; GM1 staining indicated by arrows. Scale bar is 30 μm. Row 3: low-magnification images from the thalamus (TH); thalamic neurons indicated by arrowheads; GM1 staining indicated by arrows. Scale bar is 30 μm. Row 4: GM1 accumulation (arrows) within activated astrocytes in the thalamus of normal and NPC1 brains. Scale bar is 10 μm. B: Coronal brain sections were stained with anti-GM2 antibodies (green) and neurotrace (blue) (row 1) or anti-macrophage (F4/80) antibodies (blue) (bottom panel). Row 1: faint GM2 accumulation in neurons (asterisk) of NPC1 thalamus (TH). Scale bar is 10 μm. Bottom panel: GM2 (arrowheads) accumulates in macrophages of the NPC1 thalamus. Scale bar is 3 μm. Images are representative of a large number of photographs obtained by confocal microscopy.

the thalamus (20). In the current study, we examined these same regions during the earlier stages of NPC disease from day 9 to day 22 using BCθ to detect intracellular cholesterol accumulation. As early as day 9, we observed significant cholesterol accumulation throughout all layers of the NPC cortex. In the NPC cerebellum, we observed low levels of cholesterol accumulation in both Purkinje neurons and granule neurons at day 9, with accumulation increasing to day 22. In contrast, Treiber-Held et al. reported no cholesterol accumulation in granule neurons, and did not report specific cholesterol accumulation in Purkinje neurons until 10 weeks of age, a stage at which 90% of these neurons have been lost (20). In contrast to

the findings of Treiber-Held et al., we observed significant cholesterol accumulation throughout the NPC hippocampus in both the CA1 and CA3 regions (20). In addition, at day 9, we observed significant cholesterol accumulation in the dentate gyrus, specifically within the small granule neurons of the granule layer. Interestingly, Treiber-Held et al. reported only light filipin staining in the NPC thalamus, an area reported to be the most severely affected early in NPC disease (20). Consistent with the thalamus exhibiting early neurodegeneration (1, 21), we found that the thalamus exhibited the most severe levels of BCθ staining. We attribute the differences in results between the current study and the work of Treiber-Held et al. to the superiority of BCθ staining over filipin staining (20). Our results show in vivo that although neuronal morphology may appear normal, cholesterol accumulates in virtually all neurons as early as postnatal day 9. Recently, mice lacking both NPC1 and the glycosphingolipid synthetic enzyme GM2/GD2 synthase have become available (29, 30). It will be interesting to use BCθ as the cholesterol stain to critically evaluate and compare the neuronal cholesterol accumulation in these mice and their progenitors.

Two recent studies have reported filipin-positive cholesterol accumulation in primary neurons isolated from either embryonic or early postnatal NPC mice in vitro (20, 31). From these findings, these investigators have suggested that cholesterol may accumulate in neurons in vivo even before birth. In both studies, neurons were isolated and then cultured in the absence of glial cells for 1 to 10 days to allow neurons to adhere and to regrow axons and dendrites lost during the isolation procedure. It is possible that various metabolic alterations/adaptations may occur during the re-establishment period in these neuronal cultures. Therefore, cholesterol accumulation observed in primary cultures of NPC neurons in vitro may not accurately reflect the temporal accumulation of cholesterol in vivo.

Purkinje neurons have been reported to exhibit numerous axonal and dendritic neurodegenerative alterations, with the degeneration of dendritic arbors occurring in a retrograde manner (18, 21, 32). In the current study, we report significant cholesterol accumulation as early as postnatal day 9 not only within the Purkinje cell body but also within the main dendritic branches feeding the extensive Purkinje dendritic network. These findings suggest that malfunction of the NPC1 protein leads to abnormal cholesterol distribution/accumulation within the dendritic network, which may result in cholesterol starvation at the synapse and the retrograde degeneration characteristic of Purkinje dendrites. Such a critical dependence on NPC1 for cholesterol transport may explain, in part, why degeneration of Purkinje neurons is a hallmark of NPC disease. In cultured sympathetic neurons of the peripheral nervous system, Karten et al. (9) reported that the NPC1 protein resides in the cell body as well as in the axon and that cholesterol synthesized endogenously in the neuronal cell body transports to the axon in an NPC1-dependent manner. A similar transport mechanism may exist in the extensive dendritic network of Purkinje neurons as well as in axons and dendrites of other neurons throughout the CNS in

vivo. These findings suggest that the NPC1 protein plays a critical role in the trafficking of cholesterol throughout the extensive Purkinje dendritic architecture.

In both NPC patients and NPC1 mice, the thalamus exhibits severe neurodegeneration during the early onset of the disease (1, 21). We observed some of the most severe cholesterol accumulation in NPC thalamus, suggesting that cholesterol accumulation here may correlate with neuronal injury. The presence of reactive astrocytes represents one of the earliest indications of neuronal injury events, and often occurs well before morphological alterations in neurons become detectable. In NPC thalamus at postnatal day 9, virtually all neurons exhibited significant cholesterol storage, whereas only sporadic reactive astrocytes were detected; but by day 22, the thalamus was engulfed by activated astrocytes. On the basis of the timing of the astrocyte activation event, we conclude that cholesterol accumulation in neurons of the NPC mouse occurs before significant neuronal damage appears. By day 22, astrocyte activation was also observed in the cortex, although to a milder extent, whereas the hippocampus and cerebellum exhibited only sporadic astrocyte activation. Interestingly, in addition to neurons, the activated astrocytes observed in NPC brains also exhibited progressive cholesterol accumulation within their bodies and extending processes (Fig. 5B). In monkey brain, a significant amount of the NPC1 protein has been reported to reside within astrocytic processes, and recent work from our lab has demonstrated defective cholesterol trafficking in isolated NPC astrocytes (10, 33). These findings collectively implicate the critical role of the NPC1 protein in astrocyte cholesterol transport (10, 33–36), in addition to its role in neuronal cholesterol transport.

Cholesterol and sphingolipids have high affinity toward each other and are the two major constituents of the specific lipid microdomains known as rafts (37, 38). Thus, accumulation of one raft lipid in late endosome/lysosome may lead to the trapping and accumulation of the other raft lipid (39). Puri et al. (40) have shown that the accumulation of endosomal/lysosomal cholesterol in normal human fibroblasts leads to accumulation of PM-derived glycosphingolipids in the same compartment(s); conversely, in human fibroblasts derived from patients with glycosphingolipid storage diseases, the accumulation of various glycosphingolipids in the lysosome causes secondary accumulation of cholesterol in the same compartment. In addition to biophysically interacting with other raft lipid(s), cholesterol accumulation in the degradative organelle may cause inhibition of certain critical enzyme(s) involved in the degradative pathways of various sphingolipids. An example of the latter possibility has been demonstrated by Reagan et al. (41), who showed that cholesterol accumulation caused inhibition of lysosomal sphingomyelinase activity in NPC1 mutant cells. Thus, based on results demonstrated in Figs. 1 and 2 of the current work, it is reasonable to expect that certain sphingolipids may also accumulate in various neurons of NPC mice brains in the early postnatal stages. Taniguchi et al. (28) have shown that in day 21 NPC mice, increased GM1

and GM2 immunoreactivities were evident in various regions of the brain, although the cellular origin of these signals was not determined. In addition, in the 6 week NPC cerebellum, these investigators reported increases in GM1 immunoreactivity in Purkinje neurons and astrocytes, whereas increases in GM2 immunoreactivity occurred in Purkinje neurons and macrophages (28). In the current work, we used the same antibodies used in this earlier study (28) and monitored both GM1 and GM2 immunoreactivity in WT and NPC mouse brains between postnatal days 9 and 22. From day 9 to day 22, we observed no significant accumulation of GM1 and only a mild accumulation of GM2 in NPC neurons. In contrast, by postnatal day 22, we observed a significant increase in GM1 and GM2 immunoreactivity in activated NPC astrocytes and NPC macrophages, respectively. Both of these cell types are found in increased amounts in the NPC brain in response to neuronal injury. Our findings suggest that during the early stages of NPC disease, the majority of accumulated gangliosides reside within responding inflammatory cells (reactive astrocytes and macrophages), with only minor accumulation within neurons. It remains possible that glycolipids do accumulate in neurons of NPC brains during this early time frame but are simply below the level of detectability of our GM1/GM2 antibodies. In the future, this issue should be addressed by precise mass analysis of glycosphingolipids in neurons rapidly isolated from mice brains in pure form.

We have shown that in the NPC mouse brain in vivo, neuronal cholesterol accumulation precedes neurodegeneration and neuronal cell loss. Thus, cholesterol accumulation is a marker of the primary trafficking defect in the NPC1 brain. We suggest that malfunction of the NPC1 protein causes deficiencies in neuronal and glial cholesterol transport, resulting in the accumulation of cholesterol and other lipids in the internal membranes, with concomitant cholesterol starvation at critical site(s) of the PM, i.e., lipid rafts and synaptosomal membranes. This abnormal membrane cholesterol distribution eventually leads to the initiation of the neurodegenerative cascade. In the future, the BCθ reagent may prove useful in the examination of the possible role(s) of cholesterol accumulation in disease progression in other neurodegenerative disorders, including various lysosomal lipid storage diseases.■

REFERENCES

1. Patterson, M. C., M. T. Vanier, K. Suzuki, J. A. Morris, E. Carstea, E. B. Neufeld, J. E. Blanchette-Mackie, and P. G. Pentchev. 2001. Niemann-Pick disease type C: a lipid trafficking disorder. *In* The Metabolic and Molecular Bases of Inherited Disease. C. R. Scriver, A. L. Beaudet, W. S. Sly, and D. Valle, editors. McGraw-Hill, New York. 3611–3633.

2. Carstea, E. D., J. A. Morris, K. G. Coleman, S. K. Loftus, D. Zhang, C. Cummings, J. Gu, M. A. Rosenfeld, W. J. Pavan, D. B. Krizman, J. Nagle, M. H. Polymeropoulos, S. L. Sturley, Y. A. Ioannou, M. E.

Higgins, M. Comly, A. Cooney, A. Brown, C. R. Kaneski, E. J. Blanchette-Mackie, N. K. Dwyer, E. B. Neufeld, T. Y. Chang, L. Liscum, J. F. Strauss III, K. Ohno, M. Zeigler, R. Carmi, J. Sokol, D. Markie, R. R. O'Neill, O. P. van Diggelen, M. Elleder, M. C. Patterson, R. O. Brady, M. T. Vanier, P. G. Pentchev, and D. A. Tagle. 1997. Niemann-Pick C1 disease gene: homology to mediators of cholesterol homeostasis. *Science.* **277:** 228–231.

3. Ko, D. C., M. D. Gordon, J. Y. Jin, and M. P. Scott. 2002. Dynamic movements of organelles containing Niemann-Pick C1 protein: NPC1 involvement in late endocytic events. *Mol. Biol. Cell.* **12:** 601–614.

4. Zhang, M., N. K. Dwyer, D. C. Love, A. Cooney, M. Comly, E. B. Neufeld, P. G. Pentchev, E. J. Blanchette-Mackie, and J. A. Hanover. 2001. Cessation of rapid late endosomal tubulovesicular trafficking in Niemann-Pick type C1 disease. *Proc. Natl. Acad. Sci. USA.* **98:** 4466–4471.

5. Wojtanik, K. M., and L. Liscum. 2003. The transport of LDL-derived cholesterol to the plasma membrane is defective in NPC1 cells. *J. Biol. Chem.* **278:** 14850–14856.

6. Sugii, S., P. C. Reid, N. Ohgami, H. Du, and T. Y. Chang. 2003. Distinct endosomal compartments in early trafficking of low density lipoprotein-derived cholesterol. *J. Biol. Chem.* **278:** 27180–27189.

7. Lange, Y., J. Ye, and T. L. Steck. 1998. Circulation of cholesterol between lysosomes and the plasma membrane. *J. Biol. Chem.* **273:** 18915–18922.

8. Cruz, J. C., and T. Y. Chang. 2000. Fate of endogenously synthesized cholesterol in Niemann-Pick type C1 cells. *J. Biol. Chem.* **275:** 41309–41316.

9. Karten, B., D. E. Vance, R. B. Campenot, and J. E. Vance. 2003. Trafficking of cholesterol from cell bodies to distal axons in Niemann-Pick C1-deficient neurons. *J. Biol. Chem.* **278:** 4168–4175.

10. Reid, P. C., S. Sugii, and T. Y. Chang. 2003. Trafficking defects in endogenously synthesized cholesterol in fibroblasts, macrophages, hepatocytes, and glial cells from Niemann-Pick type C1 mice. *J. Lipid Res.* **44:** 1010–1019.

11. Neufeld, E. B., M. Wastney, S. Patel, S. Suresh, A. M. Cooney, N. K. Dwyer, C. F. Roff, K. Ohno, J. A. Morris, E. D. Carstea, J. P. Incardona, J. F. Strauss III, M. T. Vanier, M. C. Patterson, R. O. Brady, P. G. Pentchev, and E. J. Blanchette-Mackie. 1999. The Niemann-Pick C1 protein resides in a vesicular compartment linked to retrograde transport of multiple lysosomal cargo. *J. Biol. Chem.* **274:** 9627–9635.

12. Liscum, L. 2000. Niemann-Pick type C mutations cause lipid traffic jam. *Traffic.* **1:** 218–225.

13. Davies, J. P., F. W. Chen, and Y. A. Ioannou. 2000. Transmembrane molecular pump activity of Niemann-Pick C1 protein. *Science.* **290:** 2295–2298.

14. Naureckiene, S., D. E. Sleat, H. Lackland, A. Fensom, M. T. Vanier, R. Wattiaux, M. Jadot, and P. Lobel. 2000. Identification of HE1 as the second gene of Niemann-Pick C disease. *Science.* **290:** 2298–2301.

15. Ko, D. C., J. Binkley, A. Sidow, and M. P. Scott. 2003. The integrity of a cholesterol-binding pocket in Niemann-Pick C2 protein is necessary to control lysosome cholesterol levels. *Proc. Natl. Acad. Sci. USA.* **100:** 2518–2525.

16. Xie, C., S. D. Turley, P. G. Pentchev, and J. M. Dietschy. 1999. Cholesterol balance and metabolism in mice with loss of function Niemann-Pick C protein. *Am. J. Physiol.* **276:** E336–E344.

17. Vanier, M. T. 1999. Lipid changes in Niemann-Pick disease type C brain: personal experience and review of the literature. *Neurochem. Res.* **24:** 481–489.

18. Zervas, M., K. Dobrenis, and S. U. Walkley. 2001. Neurons in Niemann-Pick disease type C accumulate gangliosides as well as unesterified cholesterol and undergo dendritic and axonal alterations. *J. Neuropathol. Exp. Neurol.* **60:** 49–64.

19. Zervas, M., K. L. Somers, M. A. Thrall, and S. U. Walkley. 2001. Critical role of glycosphingolipids in Niemann-Pick disease type C. *Curr. Biol.* **11:** 1283–1287.

20. Treiber-Held, S., R. Distl, V. Meske, F. Albert, and T. G. Ohm. 2003. Spatial and temporal distribution of intracellular free cholesterol in brains of a Niemann-pick type C mouse model showing hyperphosphorylated tau protein. Implications for Alzheimer's disease. *J. Pathol.* **200:** 95–103.

21. Ong, W-Y., U. Kumar, R. C. Switzer, A. Sidhu, G. Suresh, C-Y. Hu, and S. C. Patel. 2001. Neurodegeneration in Niemann-Pick type C disease mice. *Exp. Brain Res.* **141:** 218–231.

22. German, D. C., C-L. Liang, T. Song, U. Yazdani, C. Xie, and J. M.

Dietschy. 2002. Neurodegeneration in the Niemann-Pick C mouse: glial involvment. *Neuroscience.* **109:** 437–450.

23. Iwamoto, M., I. Morita, M. Fukuda, S. Murota, S. Ando, and Y. Ohno-Iwashita. 1997. A biotinylated perfringolysin O derivative: a new probe for detection of cell surface cholesterol. *Biochim. Biophys. Acta.* **1327:** 222–230.

24. Waheed, A. A., Y. Shimada, H. F. Heijnen, M. Nakamura, M. Inomata, M. Hayashi, S. Iwashita, J. W. Slot, and Y. Ohno-Iwashita. 2001. Selective binding of perfringolysin O derivative to cholesterol-rich membrane microdomains (rafts). *Proc. Natl. Acad. Sci. USA.* **98:** 4926–4931.

25. Sugii, S., P. C. Reid, N. Ohgami, Y. Shimada, R. A. Maue, H. Ninomiya, Y. Ohno-Iwashita, and T. Y. Chang. 2003. Biotinylated theta toxin derivative as a probe to examine intracellular cholesterol domains in normal and Niemann-Pick type C1 cells. *J. Lipid Res.* **44:** 1033–1041.

26. Mobius, W., Y. Ohno-Iwashita, E. G. van Donselaar, V. M. Oorschot, Y. Shimada, T. Fujimoto, H. F. Heijnen, H. J. Geuze, and J. W. Slot. 2002. Immunoelectron microscopic localization of cholesterol using biotinylated and non-cytolytic perfringolysin O. *J. Histochem. Cytochem.* **50:** 43–55.

27. Loftus, S. K., J. A. Morris, E. D. Carstea, J. Z. Gu, C. Cummings, A. Brown, J. Ellison, K. Ohno, M. A. Rosenfeld, D. A. Tagle, P. G. Pentchev, and W. J. Pavan. 1997. Murine model of Niemann-Pick C disease: mutation in a cholesterol homeostasis gene. *Science.* **277:** 232–235.

28. Taniguchi, M., Y. Shinoda, H. Ninomiya, M. T. Vanier, and K. Ohno. 2001. Sites and temporal changes of gangliosides GM1/GM2 storage in the Niemann-Pick disease type C mouse brain. *Brain Dev.* **23:** 414–421.

29. Gondre-Lewis, M. C., R. McGlynn, and S. U. Walkley. 2003. Cholesterol accumulation in NPC1-deficient neurons is ganglioside dependent. *Curr. Biol.* **13:** 1324–1329.

30. Liu, Y., Y. P. Wu, R. Wada, E. B. Neufeld, K. A. Mullin, A. C. Howard, P. G. Pentchev, M. T. Vanier, K. Suzuki, and R. L. Proia. 2000. Alleviation of neuronal ganglioside storage does not improve the clinical course of the Niemann-Pick C disease mouse. *Hum. Mol. Genet.* **9:** 1087–1092.

31. Karten, B., D. E. Vance, R. B. Campenot, and J. E. Vance. 2002. Cholesterol accumulates in cell bodies, but is decreased in distal axons, of Niemann-Pick type C1-deficient neurons. *J. Neurochem.* **83:** 1154–1163.

32. Higashi, Y., S. Murayama, P. G. Pentchev, and K. Suzuki. 1993. Cerebellar degeneration in the Niemann-Pick type C mouse. *Acta. Neuropathol.(Berl.)* **85:** 175–184.

33. Hu, C. Y., W. Y. Ong, and S. C. Patel. 2000. Regional distribution of NPC1 protein in monkey brain. *J. Neurocytol.* **29:** 765–773.

34. Patel, S. C., S. Suresh, U. Kumar, C. Y. Hu, A. Cooney, E. J. Blanchette-Mackie, E. B. Neufeld, R. C. Patel, R. O. Brady, Y. C. Patel, P. G. Pentchev, and W. Y. Ong. 1999. Localization of Niemann-pick C1 proteins in astrocytes: implications for neuronal degeneration in Niemann-Pick type C disease. *Proc. Natl. Acad. Sci. USA.* **96:** 1657–1662.

35. German, D. C., E. M. Quintero, C. L. Liang, C. Xie, and J. M. Dietschy. 2001. Degeneration of neurons and glia in the Niemann-Pick C mouse is unrelated to the low-density lipoprotein receptor. *Neuroscience.* **105:** 999–1005.

36. Mauch, D. H., K. Nagler, S. Schumacher, C. Goritz, E. C. Muller, A. Otto, and F. W. Pfieger. 2001. CNS synaptogenesis promoted by glia-derived cholesterol. *Science.* **294:** 1354–1357.

37. Simons, K., and E. Ikonen. 1997. Functional rafts in cell membranes. *Nature.* **387:** 569–572.

38. Brown, D. A., and E. London. 1998. Function of lipid rafts in biological membranes. *Annu. Rev. Cell Dev. Biol.* **14:** 111–136.

39. Simons, K., and J. Gruenberg. 2000. Jamming the endosomal system: lipid rafts and lysosomal storage diseases. *Trends Cell Biol.* **10:** 459–462.

40. Puri, V., R. Watanabe, M. Dominguez, X. Sun, C. L. Wheatley, D. L. Marks, and R. E. Pagano. 1999. Cholesterol modulates membrane traffic along the endocytic pathway in sphingolipid-storage diseases. *Nat. Cell Biol.* **1:** 386–388.

41. Reagan, J. W., Jr., M. L. Hubbert, and G. S. Shelness. 2000. Posttranslational regulation of acid sphingomyelinase in Niemann-Pick type C1 fibroblasts and free cholesterol-enriched Chinese hamster ovary cells. *J. Biol. Chem.* **275:** 38104–38110.